Damping of unbound single-particle modes

S. Fortier,[1] D. Beaumel,[1] S. Galès,[1] J. Guillot,[1] H. Langevin-Joliot,[1] H. Laurent,[1] J. M. Maison,[1] J. Bordewijk,[2] S. Brandenburg,[2] A. Krasznahorkay,[3] G. M. Crawley,[4] C. P. Massolo,[5] M. Rentería,[5] and A. Khendriche[6]

[1]*Institut de Physique Nucléaire, IN2P3-CNRS, 91406 Orsay Cedex, France*

[2]*Kernfysisch Versneller Instituut, 9747 AA Groningen, The Netherlands*

[3]*Nuclear Research Institute, Debrecen P.O. Box 51, H-4001, Hungary*

[4]*NSCL, Michigan State University, East Lansing, Michigan 48824*

[5]*Dep. Física, Fac. Cs. Exactas, UNLP, CC N° 67, 1900 La Plata, Argentina*

[6]*Institut de Sciences Exactes, Universite de Tizi-Ouzou, 15000 Tizi-Ouzou, Algeria*

(Received 21 July 1995)

The $(\alpha,{}^3\mathrm{He}\text{-}n)$ reaction has been investigated at 120 MeV incident energy on ^{64}Ni, ^{90}Zr, and ^{120}Sn target nuclei. Neutrons in coincidence with ^{3}He particles emitted at 0° were detected using the multidetector array EDEN, in order to get information about the decay of single-particle states embedded in the $(\alpha,{}^3\mathrm{He})$ continuum. Neutron angular correlations, multiplicity values, and branching ratios to low-lying states of the final nuclei have been compared with the predictions of the statistical decay model. Evidence for a significant nonstatistical decay branch has been observed in the three nuclei below about 15 MeV excitation energy. Direct branching ratios in ^{91}Zr deduced from this analysis are compared with the predictions of two nuclear structure models. At higher excitation energy, the decay characteristics of the $(\alpha,{}^3\mathrm{He})$ continuum are shown to be mainly statistical.

PACS number(s): 21.10.Pc, 25.55.Hp, 21.10.Ma, 29.30.Hs

I. INTRODUCTION

Various theoretical approaches [1–4] have attempted to describe the continuum spectra from single-nucleon stripping reactions as the sum of two contributions, one due to the elastic breakup of the projectile, and the other one resulting mainly from transfer to unbound single-particle states. In particular, semiclassical calculations using the Bonaccorso-Brink (BB) model [4] have been able to reproduce the inclusive spectra from stripping reactions induced by various hadronic probes on several medium and heavy nuclei. These spectra exhibit giant-resonance-like structures corresponding to the preferential excitation of unbound single-particle states in high-spin external orbitals, due to the selectivity of stripping reactions for large angular momentum transfer [5–7]. Typical examples are the "giant states" observed at 13 MeV in ^{91}Zr and 10 MeV in ^{209}Pb , which have been shown [5] to be mainly due to the population of the external $1i_{13/2}$ and $1k_{17/2}$ neutron orbitals, respectively.

The damping of these resonant states occurs through the mixing of the initial single-particle mode with the numerous underlying complex states with the same spin and parity. The quasiparticle-phonon model [5] describes the first step of the damping process as the coupling of the single-particle mode to surface vibrations. In the following steps, coupling to more and more complex configurations may occur until complete thermalization is reached. Information on the damping of unbound single-particle states may be obtained through the investigation of their particle decay. In particular, when the observed decay characteristics differ from those predicted for a fully thermalized system, the nonstatistical part of the decay depends on the microscopic structure of the giant state, thus providing a stringent test for theoretical calculations. Recently two different models, the quasiparticle-phonon model (QPM) [8,9] and the coupled-channel approach (CCA) [10], have been used to calculate the direct and semidirect neutron decay of high-spin single-particle states, predicting the nonstatistical branching ratios to the low-lying states of the target nuclei.

In order to investigate the damping of single-particle neutron excitations in medium-heavy mass nuclei, an extensive study of the $(\alpha,{}^3\mathrm{He}\text{-}n)$ reaction has been performed, using the neutron multidetector array EDEN [11]. Results obtained for the decay of ^{209}Pb have been reported in Ref. [12]. The present paper reports the detailed results obtained from the study of the decay properties of ^{91}Zr, since only a brief account of the neutron decay of the giant state located at 13 MeV in ^{91}Zr had been given previously in Ref. [13]. In addition, results on the decay of continuum states in ^{65}Ni and ^{121}Sn, obtained using the same experimental arrangement, are also reported. The global characteristics of the decay of these three nuclei are compared with the predictions of the statistical model, using the results of the semiclassical BB calculations as input data. Significant nonstatistical decay branches have been observed up to about 8 MeV above the neutron emission threshold. For ^{91}Zr, the results can be compared with the predictions of the QPM [9] and CCA [10] calculations.

The experimental setup and the methods used for data reduction and analysis are presented in Secs. II and III, respectively. Results obtained in the 8 MeV wide excitation energy range above the neutron emission threshold are reported in Sec. IV for ^{91}Zr and in Sec. V for ^{65}Ni and ^{121}Sn. The data obtained for the three nuclei at higher excitation energy, where the decay of the continuum states appears to be mainly statistical, will be discussed in the last section.

II. EXPERIMENTAL SET UP

The present experiment was performed using a 120 MeV α-particle beam from the AVF cyclotron at KVI Groningen. The thicknesses of isotopically enriched targets of ^{90}Zr (97.6%), ^{120}Sn (99.9%), and ^{64}Ni (96.5%) were 5.0, 5.2, and 1.5 mg/cm^2, respectively. The outgoing ^{3}He particles were analyzed by the QMG/2 magnetic spectrograph [14] placed at 0° with respect to the beam direction. The angular acceptance of the spectrometer corresponds to a solid angle of about 10 msr. The direct beam was stopped between the first and second dipole magnets. The identification of ejectiles was provided by energy loss and time of flight measurements performed using a plastic scintillator located behind the focal plane, while the position in the focal plane was measured with a multiwire drift chamber [15]. Information on the incident horizontal angle of the particle was also provided by the drift chamber, allowing the elimination of particles with trajectories originating from the beam stop. The energy calibration of the focal plane detector was done by measuring the position of peaks corresponding to the excitation of levels with accurately known excitation energies in ^{13}C and ^{17}O, using the (α,^{3}He) reaction on a mylar target. Excitation energy ranges of about 20 MeV could be investigated in a single setting of the magnetic field. The lowest excitation energies investigated in ^{65}Ni, ^{91}Zr, and ^{121}Sn were 4 MeV, 7 MeV, and 6 MeV, respectively. An experimental energy resolution of about 150 keV was obtained for the ^{3}He spectra.

Neutrons emitted between 68° and 168° to the beam direction were detected by 32 cells of the multidetector EDEN [11], located at 1.75 m from the target position in three shells, one in the reaction plane and the two others at azimuthal angles of $\pm 9°$ [12]. The individual counters are cylindrical cells, with a diameter of 20 cm and a thickness of 5 cm. In the present geometrical arrangement, the total solid angle of the neutron multidetector is 2.6% of 4π. The counters are filled with the liquid scintillator NE213, allowing pulse-shape discrimination between neutrons and γ rays. Technical details of the neutron multidetector and its associated electronics are given in Ref. [11].

Neutron energies E_n were obtained from the time of flight measurement, deduced from the timing signals in the NE213 cell, the focal plane plastic scintillator, and the rf signal of the cyclotron. The beam intensity had been limited to about 2 *nA* in order to keep the ratio of true to random coincident events around 2.5. The present experimental setup provided a neutron energy resolution ranging from 60 keV at 1 MeV to 500 keV at 6 MeV, as measured in the calibration runs performed with a Mylar target [11]. Under these conditions, the first excited states of the final nuclei under investigation are well resolved, as will be shown below. For unresolved multiplets of final states at higher excitation energy, complementary data were obtained using a large volume (80%) Ge detector placed at 90° and about 25 cm from the target position. In spite of the low statistics, it was possible to accurately measure the energies of some of the coincident γ rays emitted during the decay process after neutron emission, thus giving information on the final states involved in the decay process.

The absolute efficiency $\epsilon(E_n)$ of each detector cell has been previously [11] determined for a 60 keV electron-equivalent energy threshold. Values higher than 0.30 are obtained for neutron energies below 6 MeV. In order to monitor electronic fluctuations which could modify the value of the effective threshold, the calibration of each detector was checked at different stages of the experiment with the 60 keV γ ray from an ^{241}Am source. The relative uncertainty on the efficiency values has been estimated to be lower than about 7% for neutron energies above 1 MeV and 15% for the 0.5–1 MeV energy range. Only neutron energies above 0.5 MeV have been taken into account, as the efficiency of the EDEN cells is not accurately known below this energy [11].

Multiparameter events corresponding to a coincidence between the focal plane plastic scintillator and the EDEN or Ge detectors were registered on magnetic tape, together with scaled-down singles events for absolute normalization of coincident data. After subtraction of random events and correction for detection efficiency, the spectra of neutrons emitted from the initial nucleus at excitation energy E_{x_a} can be displayed as a function of the missing energy E_{x_b}, defined by $E_{x_a} - E_n(\text{c.m.}) - S_n$, S_n being the one-neutron emission threshold. In the case of one-neutron emission, E_{x_b} is the excitation energy of the final level in the target nucleus which is fed by the neutron decay.

III. DATA ANALYSIS

A. Semiclassical description of the inclusive (α,^{3}He) spectra

The singles (α,^{3}He) spectra measured for the three target nuclei are displayed in Fig. 1. The giant states observed around 13 MeV in ^{91}Zr and 6 MeV in ^{121}Sn in previous studies of the same reaction at 183 MeV incident energy [5,16] are also strongly excited at 120 MeV, as seen in these spectra measured above the neutron emission threshold. There was no previous data on the high-lying single-particle states in ^{65}Ni. Above the region of discrete levels or groups of levels (0–9 MeV), the present spectrum exhibits a broad structure centered at about 11 MeV.

These inclusive spectra are compared in Fig. 1 with the predictions of the semiclassical BB model [4], normalized to the data. This model calculates spectra observed in transfer reactions as the sum of an absorptive part and an elastic breakup part, deduced from the S matrix describing the neutron-target nucleus interaction [3]. In the present calculation, the parameters of the optical potentials used for the three nuclei have been adjusted in order to best reproduce the inclusive spectra [4].

The calculated contributions of the predominant (l,j) wave functions to the absorption cross sections are shown in Fig. 2 as a function of excitation energies. The predictions for ^{91}Zr and ^{121}Sn are in qualitative agreement with the proposed [5,16] origin of the giant states in these nuclei, as discussed below. The structure observed around 11 MeV in ^{65}Ni [Fig. 1(c)] both in the experimental and calculated spectra is probably due predominantly to the excitation of the $h_{11/2}$ resonant state, as shown by the results of the semiclassical calculations of Bonaccorso [4] reported in Fig. 2(c). These predictions for the contributions of various spin values in the (α,^{3}He) continuum will be used as input data in the statistical calculations and in the analysis of angular correlations.

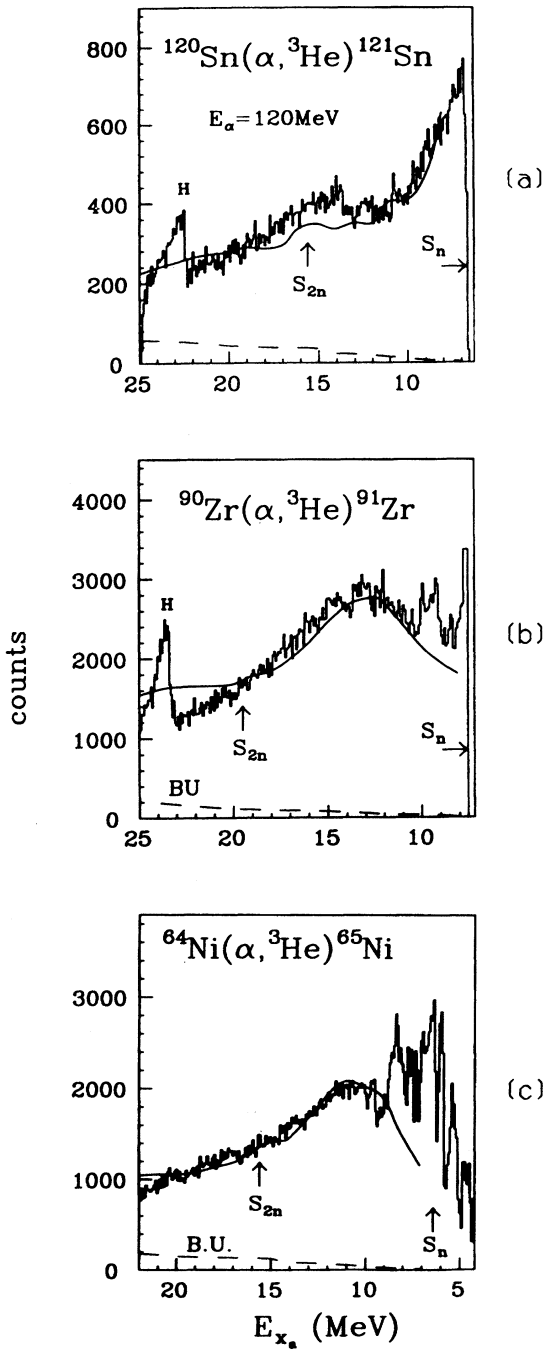

FIG. 1. Singles (α,^{3}He) spectra measured at 0° and 120 MeV incident energy on ^{64}Ni, ^{90}Zr, and ^{120}Sn target nuclei. The peak labeled with "H" comes from the hydrogen contaminant. The total (absorption+breakup) calculated spectra [4] using the semiclassical Brink-Bonaccorso (BB) model (full lines) are shown for comparison. The breakup (BU) part of the calculated spectra is indicated by the dashed lines.

On the other hand, the BB calculations predict only a weak contribution of elastic breakup to the inclusive (α,^{3}He) cross sections. The theoretical partial breakup cross sections for the three target nuclei are shown as dashed lines in Fig. 1. These predictions will be compared in Sec. VI with the results of the exclusive data measured in the high excitation energy region.

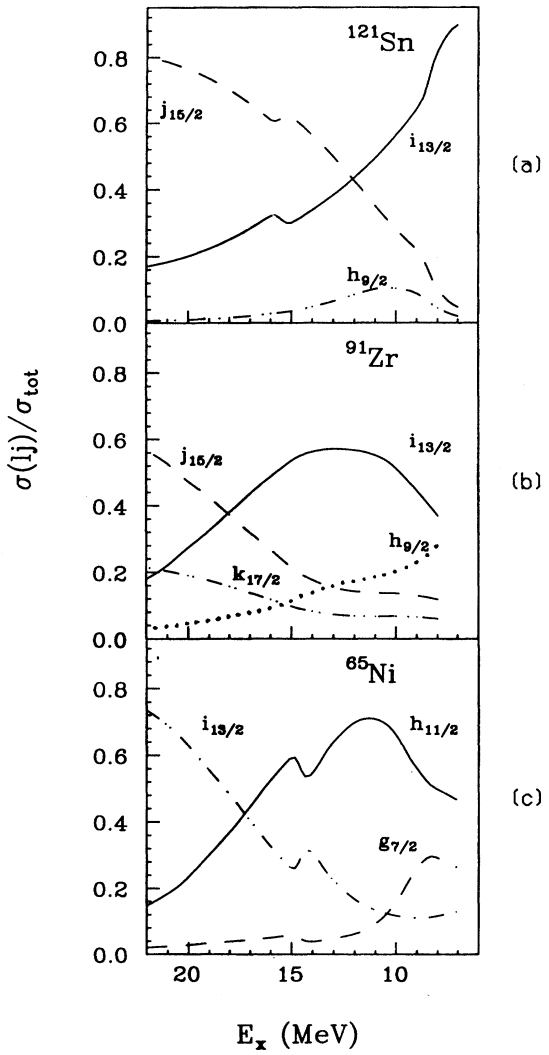

FIG. 2. Spin distributions of final states in ^{65}Ni, ^{91}Zr, and ^{121}Sn excited by (α,^{3}He) reaction at 120 MeV, as predicted by the semiclassical model of Brink and Bonaccorso [4].

B. Angular correlation analysis

For a transition from an energy bin around E_{x_a} in the initial nucleus to a final level or group of levels around energy E_{x_b}, the neutron yield $y(\theta)$ is defined as the ratio of the number of coincident events $n(\theta)_{a\to b}$ to the corresponding number of singles events n_s. The $n(\theta)_{a\to b}$ value has been corrected for the absolute efficiency of the detector and expressed in the center of mass frame of the emitting nucleus. Due to the present cylindrical geometry provided by the detection of the ejectile around 0°, $y(\theta)$ can be expressed by a sum of Legendre polynomials:

$$y(\theta)=\sum_k A_k P_k(\cos\theta)=B_{\exp}W(\theta), \qquad (1)$$

where $W(\theta)$ is the normalized angular correlation and $B_{\exp}$ is the branching ratio at energy E_{x_a}, as given by the coefficient A_0 of the correlation.

The general formulation of the particle angular correlation $W(\theta)$ for a transition from an isolated level with spin J_a to a final level with spin J_b may be found in Ref. [17]. The correlation is symmetric with respect to 90° and can be expressed by a sum of even Legendre polynomials with a maximum rank $k_{\max}$ depending on the spin values.

Theoretical angular correlations for each possible $(J_a \rightarrow J_b)$ transition have been calculated using the code CORELY [18]. Ingredients of these calculations are the statistical tensors describing the alignment of the emitting states and the relative amplitudes and phases of the various possible (lj) partial waves participating to the decay process. It has been assumed that no interference occurs between partial waves, and that their relative contributions are proportional to the transmission coefficients T_{lj}, calculated using the neutron optical potential of Rapaport *et al.* [20]. Statistical tensors averaged over the finite solid angle of the spectrometer were deduced from the $(\alpha,{}^3\mathrm{He})$ reaction amplitudes, calculated using the distorted wave Born approximation (DWBA) code DWUCK4 [19], with the same optical model parameter sets as in Ref. [12].

Angular correlations measured in the continuum result from the decay of several states with different J_a values and thus correspond to the weighted sum of the individual J_a contributions, with relative strengths proportional to the relative inclusive cross sections $\sigma_{J_a}/\sigma_{\mathrm{tot}}$, here assumed to be equal to the predicted values displayed in Fig. 2. Possible interference between emitting states with opposite parity was neglected. The resulting theoretical angular correlations which are presented in the next sections have been further normalized to the data.

The values of the experimental neutron branching ratios $B_{\exp}$ corresponding to each 0.5 MeV energy bin of the initial nucleus were extracted from $y(\theta)$ by a least square fitting procedure where all even values of $k_{\max}$ up to 16 have been considered. Within the error bars, $B_{\exp}$ was found to be nearly independent of the value of $k_{\max}$, for $k_{\max}$ greater or equal to 4. By summing the $B_{\exp}$ values over all neutron energies above the 0.5 MeV experimental threshold, one gets the experimental neutron multiplicity M_n.

The validity of the present analysis, assuming a neutron emission symmetric relative to 90°, has to be checked by examining the experimental angular correlations $W(\theta)$. Possible sources of asymmetry are interferences between decaying states with opposite parity and a non-negligible contribution of the breakup process to the inclusive cross sections. This will be discussed below.

C. Statistical model calculations

In order to compare the decay characteristics of the $({}^3\mathrm{He},\alpha)$ continuum with those expected from the decay of a completely equilibrated nucleus, statistical calculations have been performed using the code CASCADE [21], which is based on the Hauser-Feshbach formalism. Neutron spectra, as well as branching ratios, were calculated for each 100 keV excitation energy bin E_{x_a} in the emitting nucleus. These calculated spectra expressed as function of final energy E_{x_b} were further folded with the experimental energy resolution, with suppression of neutron energies below the 0.5 MeV threshold, and summed over E_{x_a} energy bins of 1 MeV. The calculated spectra were normalized to the experiment using the standard procedure generally adopted in the studies of particle decay of giant resonances [22], viz. by assuming that the contribution of the statistical decay process is the *maximum* possible one, so that the statistical spectra do not exceed the corresponding experimental ones anywhere. For the high excitation energy range of decaying nuclei, this condition is usually fulfilled by adjusting the normalization factor so that the spectra coincide at low neutron energy.

The statistical decay of a thermalized system is entirely determined by the transmission coefficients, the spin distribution in the initial nucleus, and the level densities in the neighbouring nuclei. Neutron transmission coefficients were deduced from the optical potential from Rapaport *et al.* [20]. The initial spin distributions used in the present calculations are those previously shown in Fig. 2. All known discrete levels in the final nuclei up to an upper energy limit equal to 2.8 MeV in ^{64}Ni and ^{120}Sn, and 4.8 MeV in ^{90}Zr were taken into account in the calculations. Above the region of discrete levels, the parametrization of level densities in the code CASCADE [21] uses the analytical form of the back-shifted Fermi gas model. Standard level density parameters taken from Dilg *et al.* [23] were adopted as input data, with the exception of the parameter a. This parameter was in fact allowed to vary with energy in a linear way, in order to best reproduce the shapes of the experimental neutron spectra observed in coincidence with the high excitation energy region, supposed to be mostly statistical. Another requirement for the choice of a was to avoid discontinuities in the intermediate energy region above the known discrete levels, given as input data for the calculation. The values of the level density parameter a deduced from this analysis are close to the standard Dilg values [23] for the tin and nickel target nuclei. On the other hand, the energy spectra of neutrons from zirconium can only be reproduced by statistical calculations if one chooses empirical a values in ^{90}Zr linearly decreasing with decreasing energies, from a value of 11 at 13 MeV to 7 at 5 MeV.

Due to the angular momentum selectivity of the $(\alpha,{}^3\mathrm{He})$ reaction and the generally low angular momentum carried by the decay neutron, the statistical decay preferentially populates levels with spin values between about 6 and 10. The present results indicate that the corresponding level density in ^{90}Zr is significantly overestimated by the standard back-shifted Fermi gas parametrization of CASCADE, which extrapolates the density of low spin levels determined by Dilg to higher spin values. Similar conclusions about the necessity to modify the standard input data in CASCADE had been drawn in the case of ^{208}Pb in our previous paper [12]. At low excitation energy, it is likely that the level density is strongly dependent on shell effects, especially in magic nuclei such as ^{90}Zr and ^{208}Pb. It may be noted that experimental studies of inelastic neutron scattering at low incident energy have shown that the Fermi gas parametrization is not well suited to describe the level density for nuclei near shell closures [24].

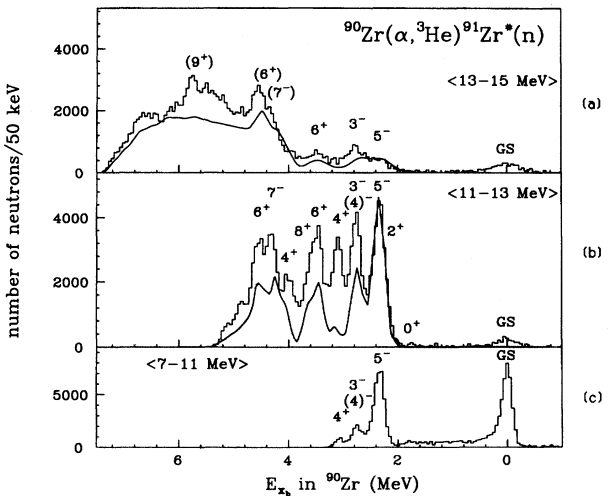

FIG. 3. Neutron spectra (histograms) from the decay of three energy bins in ^{91}Zr between 7 and 15 MeV excitation energy, displayed as a function of the energy of the residual ^{90}Zr nucleus. They are corrected for detector efficiency in order to be compared with the predictions of the statistical model (solid lines).

IV. DECAY OF UNBOUND HIGH-SPIN SINGLE-PARTICLE STATES IN ^{91}Zr ($E_x < S_n + 8$ MeV)

A. Decay spectra

Experimental neutron spectra corresponding to the decay of three energy bins between the neutron emission threshold and 15 MeV are shown in Fig. 3. In the lowest energy interval (7–11 MeV), some narrow structures have been observed in the inclusive ^{90}Zr(α,^{3}He) spectrum of Fig. 1(b), whereas the 11–13 MeV and 13–15 MeV energy bins respectively correspond to the low and high excitation energy parts of the 13 MeV giant state, shown in Ref. [5] to be predominantly due to the excitation of the $i_{13/2}$ single-particle orbital.

The neutron spectra are displayed in Fig. 3 as a function of the final energy E_{x_b}, in order to illustrate the evolution of the population of the different low-lying states in ^{90}Zr with the excitation energy of the emitting states. The good energy resolution of the multidetector for low energy neutrons allows us to identify without ambiguity most of the ^{90}Zr states which are fed by the decay of ^{91}Zr in the 7–13 MeV energy range, as seen in Figs. 3(a) and 3(b). In particular, one observes a strong peak corresponding to the 5^- state at 2.32 MeV, an unresolved peak at 2.74 MeV with mixed contributions of the lowest 3^- and 4^- states, separated by only 10 keV, and transitions to the 4^+, 6^+, and 8^+ states at 3.08, 3.45, and 3.59 MeV, respectively. Peaks observed between 4 and 6 MeV excitation energy in Figs. 3(b) and 3(c) are multiplets of levels, with predominant excitation of known [26] ^{90}Zr states with spin values 6^+, 7^-, and 9^+.

Additional information about the decay properties of ^{91}Zr may be obtained using the γ-ray data provided by EDEN and the associated germanium detector. The spectrum of ^{3}He particles in coincidence with the γ rays detected by the EDEN counters is displayed in Fig. 4(a). Above 10 MeV excitation energy, the exclusive γ-cross section exhibits a broad bump which is centered at about 16 MeV, but the

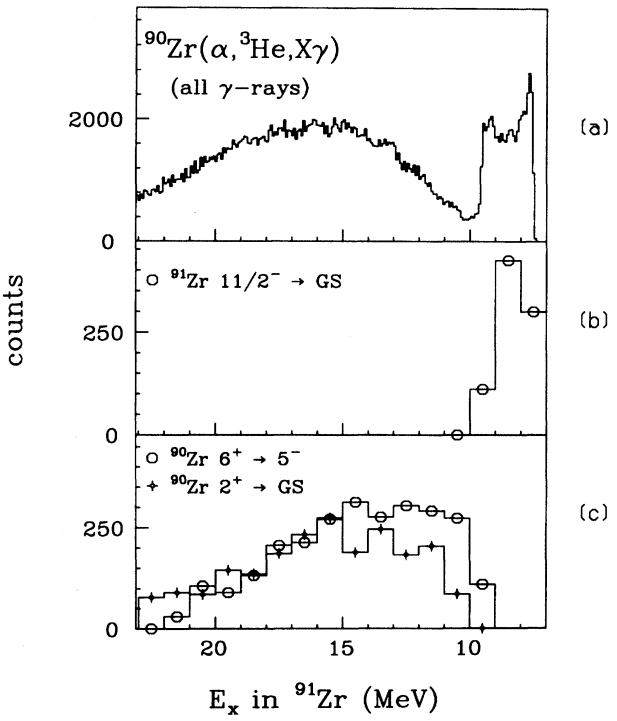

FIG. 4. ^{90}Zr(α,^{3}He)^{91}Zr spectra at 0° (a) in coincidence with γ rays detected by EDEN, (b) in coincidence with the 2170 keV γ rays from ^{91}Zr, detected by the germanium detector, and (c) in coincidence with the 1128 keV or 2188 keV γ rays from ^{90}Zr.

striking feature is the steep increase of the number of γ rays observed below 9.5 MeV. In this region, decay to the ^{90}Zr ground state is the only open neutron channel and the present data exhibits the persistence of significant γ decay well above the neutron threshold. The observed γ decay ceases with the opening of the neutron decay channel to the 5^- state, which can be readily explained by the large mean-spin value of ^{91}Zr states populated by the (α,^{3}He) reaction and centrifugal barrier effects on neutron emission at low energy. The low efficiency of the germanium detector for high energy γ-ray did not allow us to accurately determine the decay sheme in ^{91}Zr. However one can observe in the coincident γ-ray spectrum a strong secondary 2170 keV transition from the $h_{11/2}$ state to the ground state, which takes place at the end of the decay cascade. Its yield is shown in Fig. 4(b) as function of excitation energy.

Above 10 MeV, the strongest γ rays in coincidence with ^{3}He particles correspond to the known 2186 keV ($2^+ \rightarrow 0^+$) and 1129 keV ($6^+ \rightarrow 5^-$) transitions in ^{90}Zr. The corresponding intensity of γ rays measured for each 1 MeV excitation energy bin is shown in Fig. 4(c). One may note that the isomeric ($T_{1/2} = 0.8$ s) secondary ($5^- \rightarrow 0^+$) transition, which is presumably predominant in the present reaction, could not be observed in the coincident γ-ray spectrum. Other weaker transitions such as ($3^- \rightarrow 2^+$) and ($4^- \rightarrow 5^-$) were also observed over a large excitation energy range. Most of these γ rays correspond to secondary transitions, following the decay of the higher-lying ^{90}Zr states fed by the neutron emission from ^{91}Zr, as suggested by the comparison with the neutron decay data.

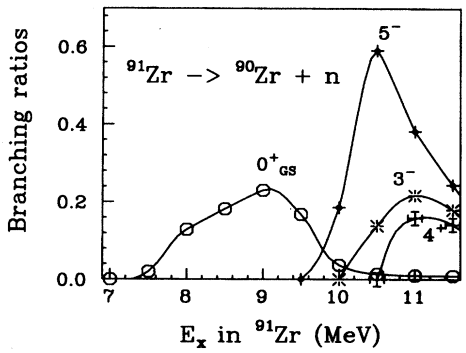

FIG. 5. Neutron branching ratios from the decay of ^{91}Zr states excited by the (α,^{3}He) reaction below 11 MeV excitation energy.

B. The low-energy (7–11 MeV) region in ^{91}Zr

Neutron branching ratios to the 0^+ ground state and low-lying excited states measured in this excitation energy region are shown in Fig. 5. Below 9.5 MeV the low branching ratio B_{GS} measured for neutron emission to the 0^+ ground state leads to the conclusion that the γ-ray emission observed in this region (see Fig. 4) corresponds to more than 75% of the inclusive (α,^{3}He) cross section. As stated above, the centrifugal barrier for low-energy neutrons strongly inhibits the neutron decay for the largest transferred angular momenta: for example, at 9 MeV excitation energy, the neutron branching ratio predicted by statistical calculations for $i_{13/2}$ states is only 2×10^{-3}, whereas it amounts to 0.50 for $h_{9/2}$. Therefore the results of statistical calculations in this low-energy range strongly depend on the assumed distribution of initial spin values. The calculations using the BB distribution of Fig. 2 have been found to underpredict the ground state branching ratio by a factor of about 3, but only slight modifications of the distribution of the weakly excited low spin components in the inclusive cross section could allow us to reproduce the data. Thus the extraction of nonstatistical branching ratios following the procedure of Sec. III C would not be significant in this region.

The angular correlation of neutrons feeding the ^{90}Zr ground state is shown in Fig. 6(a). It is rather well reproduced by the calculation described in Sec. III B (solid line) using the spin distribution of Fig. 2. The prediction for the decay of a pure $i_{13/2}$ state is shown for comparison as dashed line, in order to illustrate the sensitivity of theoretical ground state angular correlations to the mean spin value.

C. The 13 MeV giant state in ^{91}Zr

1. Experimental branching ratios

Neutron branching ratios measured for the decay of the 13 MeV giant state in ^{91}Zr to low-lying states in ^{90}Zr are plotted in Fig. 7 as a function of excitation energy. They were determined following the procedure reported in Sec. III B, using angular correlation data. A good statistical accuracy on the B_{exp} values has been obtained for the transitions to the 0^+ ground state, the 5^- state at 2.32 MeV, the (3^--4^-) unresolved doublet at 2.74 MeV, the 4^+ state at 3.08 MeV and the doublet of 6^+ and 8^+ states around 3.5 MeV, which can be observed as well-separated peaks in Fig. 3(b).

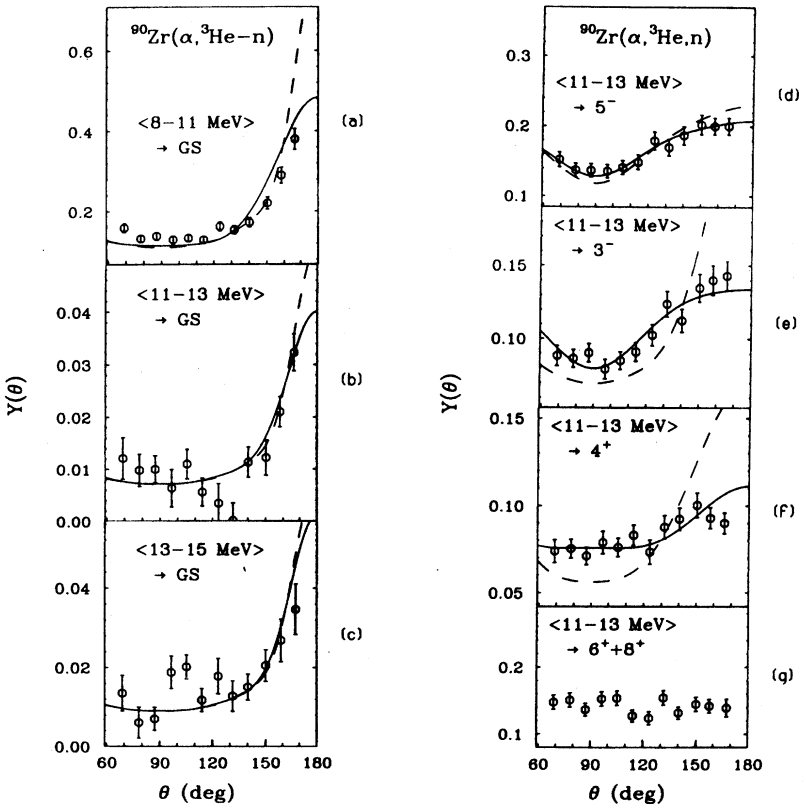

FIG. 6. Neutron angular correlations measured in ^{91}Zr. They are compared with the results of calculations for a decaying state with spin $J=13/2$ (dashed line), and a mixing of states with different J values, assuming the relative contributions from the BB model plotted in Fig. 2 (solid line).

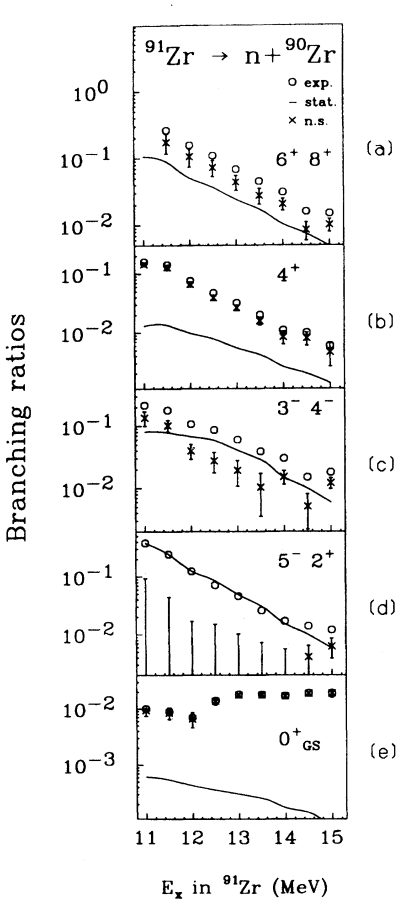

FIG. 7. Neutron branching ratios from the decay of ^{91}Zr states excited by the (α,^{3}He) reaction in the region of the 13 MeV resonant structure. Experimental branching ratios (circles) are compared with the predictions of the statistical model (dotted line). The deduced nonstatistical branching ratios (see text) are shown as crosses with error bars.

The $B_{\rm exp}$ value of the 5^- transition includes the contribution of that to the neighboring 2^+ state, estimated to be less than 20% by the multipeak analysis of the decay spectra in Fig. 3. On the other hand, the coincident γ-ray spectra from the Ge detector have shown that the contribution of the 4^- state in the decay cascade could not be neglected, but it was not possible to determine the relative weights of 3^- and 4^- states in the transition to the 2.74 MeV doublet. One observes a decrease of the experimental branching ratios with excitation energy, with the noticeable exception of the weak ground state decay for which the $B_{\rm exp}$ value increases by a factor of 3 from 12 MeV to 15 MeV.

The ground state angular correlations measured for the two energy bins are shown in Fig. 6 and compared with theoretical predictions using the BB spin distribution from Fig. 2. The calculations predict a strong backward peaking related to the high spin values of the emitting states, which is observed experimentally. However, the oscillatory behavior of the correlation around 105° for the higher energy region (13–15 MeV) cannot be accounted for by the present calculation related to neutron decay, suggesting that another process could weakly contribute to the yield of ground state neutrons. The low-energy tail of the elastic breakup process might be the origin of both the perturbed angular correlation and the increase of the $B_{\rm exp}$ value above about 13 MeV [cf. the predicted shape of the breakup contribution in Fig. 1(b)]. This could lead to some overestimation of the ground state branching ratio in that energy region. Such a contamination of the ground state angular correlation by elastic breakup becomes more apparent at higher excitation energies, as will be shown in Sec. VI.

The angular correlations measured for the neutron decay of the 13 MeV structure to the four groups of low-lying excited states in ^{90}Zr quoted above are displayed in the right part of Fig. 6. The angular correlation of neutrons feeding the (6^+, 8^+) group at 3.5 MeV [see Fig. 6(g)] is almost isotropic as transitions from the initial high spin states feeding these final states predominantly involve neutrons with low angular momenta. For final states with lower spin values, thus involving higher l transitions, anisotropic angular correlations are expected. This anisotropy is experimentally observed in Figs. 6(d)–6(f) for the transitions to the states at 2.32 MeV (5^-), 2.74 MeV (3^-,4^-) and 3.08 MeV (4^+). The results are compared with the theoretical angular correlations calculated following the procedure reported in Sec. III B. In particular, the calculated correlations shown in Fig. 6(f) correspond to the excitation of the 3^- final state alone. Theoretical calculations for a pure $i_{13/2}$ emitting state (dashed lines) cannot reproduce the data. On the other hand, very good agreement is observed using the distribution of spins from the BB calculations, with 60% of $i_{13/2}$ and about 15% of both $h_{9/2}$ and $j_{15/2}$. Therefore one may conclude that the basic assumptions of the present calculations—validity of semiclassical expectations of spin distributions, direct nature of the decay and absence of interferences between partial waves—are reasonably fulfilled at these excitation energies.

2. *Nonstatistical branching ratios*

The neutron spectra corresponding to the decay of the low (11–13 MeV) and high (13–15 MeV) energy parts of the giant state are shown in the middle and top of Fig. 3, respectively. They are compared with the spectra predicted for a fully statistical decay, normalized following the procedure reported in Sec. III C. In the present case, the calculations predict a large decay branch to the 5^- state at 2.32 MeV, so that the statistical spectra shown in Fig. 3 have been normalized to the data using this particular transition. Whereas the observed decay to the 5^- state may be interpreted as fully statistical, a significant excess of neutrons over the statistical predictions can be observed in Fig. 3 for most final low-lying states, indicating the existence of a direct decay mode for the 13 MeV giant state. In particular, the ground state transition is found to be purely nonstatistical, as the statistical contribution is about two orders of magnitude smaller than the experimental branching ratio.

The branching ratios corresponding to the nonstatistical neutrons observed in excess of the calculated spectra are given by the relation

$$B_{ns}=B_{\rm exp}-FB_{\rm calc}. \tag{2}$$

In this equation, $B_{\rm calc}$ is the branching ratio calculated by CASCADE for a fully statistical decay, and the damping factor

TABLE I. Experimental and nonstatistical neutron branching ratios of the 13 MeV giant state in ^{91}Zr, integrated over the 11–15 MeV energy range. The data are compared with the results of QPM [9] and CCA [10] theoretical calculations. In the two last columns, branching ratios are normalized over the sum of B_{ns} values for the states below 3.5 MeV (see text).

E_{x_b}	J^π (MeV)	B_{exp} (%)	B_{ns} (%)	B_{CCA} (%)	$B_{ns}/\Sigma B_{ns}$ (%)	$B_{\text{QPM}}/\Sigma B_{\text{QPM}}$ (%)
0	0^+	1.4±0.2	1.4±0.2	1.6	9±3	2.2
2.32	5^-+2^+	9.5±0.2[a]	≤1.8	0.4[b]	≤11	34
2.74	3^-+4^-	7.7±0.3[c]	3.7±0.9	2.1[d]	24±11	15
3.08	4^+	5.1±0.2	4.5±0.5		29±11	15
3.50	6^++8^-	8.8±0.2	5.6±1.8		38±11	33

[a]The contribution of the decay to the 2^+ state at 2.19 MeV is lower than 20%, according to a multipeak fitting analysis.
[b]Only for the 5^- decay channel.
[c]A sizeable contribution of the 4^- state is present, according to the analysis of γ-ray data.
[d]Only for the 3^- decay channel.

F is the fraction of inclusive cross section decaying by statistical emission. This factor F deduced from the present normalization assumption of *maximum* possible ratio of statistical over experimental decay was found to vary from 0.57 at 11 MeV to 0.82 at 15 MeV. The values of FB_{calc} calculated for the transitions to the five lowest ^{90}Zr states or groups of states are shown in Fig. 7, as function of excitation energy in ^{91}Zr, together with the nonstatistical branching ratios B_{ns} deduced from Eq. (2).

Uncertainties in the B_{ns} values may come both from the statistical calculation itself, if B_{calc} significantly depend on the particular choice of the input parameters of CASCADE, and from the normalization procedure giving the factor F to be used in Eq. (2). The error bars on the B_{ns} values plotted in Fig. 7 were evaluated from the dispersion of calculated values using another set of neutron transmission coefficients [25], and another initial spin distribution (in this case assumed to be limited to the predominant $i_{13/2}$ contribution) and in addition assuming a 10% uncertainty on the factor F. The results are summarized in Table I, giving both experimental and nonstatistical branching ratios for the 13 MeV giant state, averaged over the 11-15 MeV energy range.

However, the above assumption of subtracting the maximum possible statistical contribution $F_{\text{max}}B_{\text{calc}}$ in Eq. (2) may be questionable in the present case, where the normalization of calculated spectra relative to experiment is not done on the continuum part of low-energy neutrons as in the standard situation encountered at higher excitation energies. The effect of a possible overestimation of F on the resulting nonstatistical branching ratios has been examined. For example, by reducing F by 30%, the B_{ns} value for the 5^- channel integrated over the 11–15 MeV energy range would become equal to (2.5± 1.8)% instead of being consistent with 0, whereas the differences for the other decay branches in Table I would be within existing error bars.

3. *Comparison with theoretical calculations*

The direct neutron decay of the high-spin $h_{9/2}$, $i_{13/2}$, and $j_{15/2}$ single-particle resonant states to the ground state and low-lying collective states in ^{90}Zr has been calculated using two different theoretical approaches, which have been described respectively in Refs. [8,9] for the QPM and in Ref. [10] for the CCA.

Both the CCA and QPM calculations predict the nonstatistical neutron branching ratios B_a for each single-particle state a as a function of excitation energy. In order to compare the theoretical predictions with experimental data, which contain the contributions of several single-particle resonances, global branching ratios B have to be deduced from the weighted sum of the B_a values, using the relation

$$B=\sum_a p_a B_a . \tag{3}$$

The relative excitation probabilities p_a of the different states $h_{9/2}$, $i_{13/2}$, and $j_{15/2}$ in the inclusive $(\alpha,{}^3\text{He})$ spectrum have been evaluated by multiplying the predicted strength function by the corresponding excitation cross section calculated using the DWBA code DWUCK4 [19]. The theoretical branching ratios have been further averaged over the 11–15 MeV energy range, in order to be compared with experimental B_{ns} values.

The CCA calculations [10] use an optical potential and the simplest version of the coupled-channel approach to describe the decay to the 0^+ ground state and the collective 3^- and 5^- states, which are characterized by their deformation parameter β_L. The branching ratio B_a is defined as $\Gamma^{\uparrow}_{a\to b}/\Gamma^{\downarrow}$, with $\Gamma^{\uparrow}_{a\to b}$ and $\Gamma^{\downarrow}$ being the partial escape width to the state b and the spreading width, respectively. By assuming that the spreading width is approximately equal to the total width, the theoretical branching ratios B_{CCA} may be compared with the corresponding experimental B_{ns} values. This comparison is done in Table I, which displays a rather good agreement between theory and experiment.

In the QPM calculations [8,9] the wave functions of the low-lying final states are deduced from random-phase approximation (RPA) calculations, and decay to weakly collective states such as the lowest 4^- and 8^+ levels can be treated on the same footing as the one to the 3^- and 5^- states. Here the branching ratios B_a are defined as the ratio of the partial escape width over the total escape width

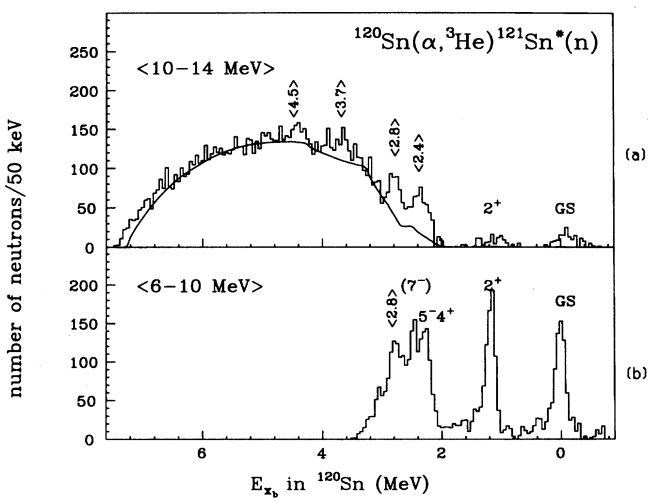

FIG. 8. Neutron spectra (histogram) from the decay of the 6–10 MeV and 10–14 MeV energy bins in ^{121}Sn (left), displayed as a function of the energy of the residual nucleus. Corresponding spectra predicted by statistical model calculations (solid lines) are also shown for comparison.

$\Sigma_b \Gamma^{\uparrow}_{a\to b}$. The branching ratios B_{QPM} averaged over the 11–15 MeV interval were deduced from Eq. (3). They cannot be directly compared with the data as they are normalized to $\Gamma^{\uparrow}$ and not to the total width Γ. The comparison between calculations and experiment can be made using ratios of branching ratios for transitions to the well-identified states below 3.7 MeV. The $B_{ns}/\Sigma B_{ns}$ are given in Table I, together with the corresponding values from the QPM calculations.

Although the QPM model predicts a predominant coupling of the single-particle mode to the low-lying collective states, one has to note the strong decay branches calculated for transitions to final states with only low collectivity (the 4^-, 6^+, and 8^+ states), which are explained by penetrability effects [9]. Rather good agreement with the data is in fact observed for the transitions to the final levels at 2.74 MeV (3^--4^-), 3.08 MeV (4^+), and 3.50 MeV (6^+-8^+). On the other hand, the predicted values for the ground state and 5^- transitions strongly disagree with the experimental results. Part of the discrepancy for the ground state transition, with theoretical value about four times weaker than observed experimentally, could come from a possible overestimation of B_{ns} due to some contribution of elastic breakup to the neutron yield. A strong direct transition to the 5^- state has been predicted by the QPM model, in contradiction with the present results showing that the data can be almost fully accounted for by statistical decay. The reason for the factor 3 difference observed in Table I between the calculated value and the upper limit given by the present statistical analysis is not well understood.

V. DECAY OF UNBOUND HIGH-SPIN SINGLE-PARTICLE STATES IN ^{121}Sn AND ^{65}Ni (E_x<S_n+8 MeV)

A. The 6–14 MeV region in ^{121}Sn

The main feature of the inclusive (α,^{3}He) spectrum displayed in Fig. 1(a) is the strongly decreasing cross section from the 6 MeV low excitation energy limit up to about 10 MeV. This 6–10 MeV region corresponds to the high-energy tail of the broad structure previously observed at 183 MeV incident energy [16]: From the DWBA analysis of ^{3}He angular distributions, it was concluded that the structure mainly originates from the selective excitation of the $i_{13/2}$ orbital, with some additional contributions of the neighbouring $h_{9/2}$ and $2f$ subshells. The spectrum of Fig. 1(a) also exhibits a higher-lying, broader and weaker structure centered at about 14 MeV, which is not well reproduced by the BB calculations. At this energy, the model predicts that $j_{15/2}$ and $i_{13/2}$ excitations contribute to 60% and 30% of the transfer cross section, respectively (see Fig. 2). Above 14 MeV, the inclusive cross section decreases in a linear monotonic way.

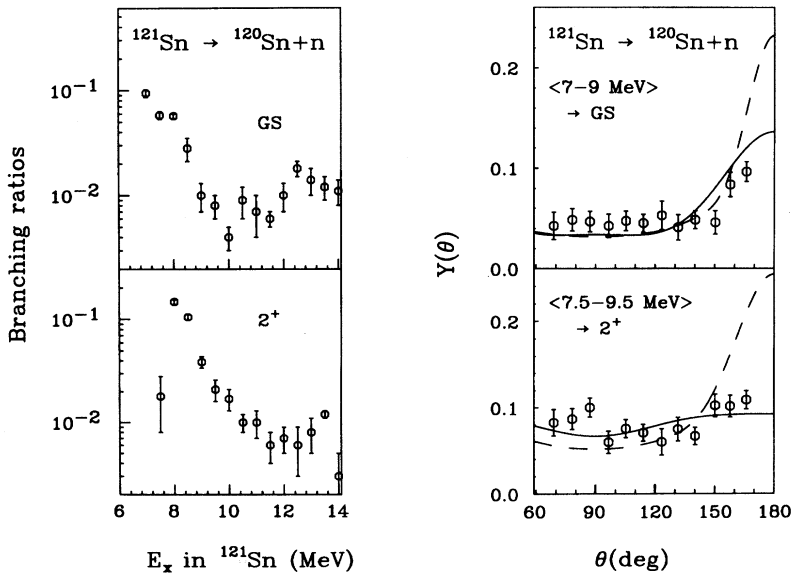

FIG. 9. Left part: neutron branching ratios to the ground state and first 2^+ state in ^{120}Sn, as a function of excitation energy in ^{121}Sn; right part: neutron angular correlations measured for the transitions to the ground state and first 2^+ state in ^{120}Sn, compared with the results of calculations for emitting states with relative J_a contributions predicted by the BB model (full lines) and one decaying state with J_a equal to 13/2 (dashed lines).

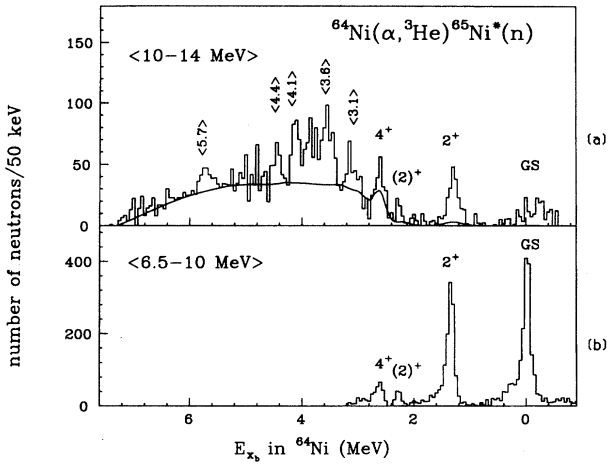

FIG. 10. Same as Fig. 9 for ^{65}Ni.

The neutron spectra displayed in Fig. 8 show the decay of two 4 MeV wide excitation energy bins in ^{121}Sn between the neutron emission threshold and 14 MeV. In addition to the well resolved 0^+ ground state and 2^+ state at 1.17 MeV, decay branches to the 4^+, 5^-, and 7^- states at respectively 2.19 MeV, 2.28 MeV, and 2.48 MeV in ^{120}Sn are clearly observed in Fig. 8(b), together with a transition to final levels around about 2.8 MeV. The decay spectrum obtained for the 10–14 MeV region is compared with statistical predictions in Fig. 8. A nonstatistical decay is clearly observed for the transitions to the ground state and 2^+ state, and also for groups of levels located around 2.4, 2.8, 3.7, and 4.5 MeV in ^{120}Sn.

The experimental branching ratios to the ground state and first 2^+ state of the target nucleus are shown in Fig. 9 (left) as function of initial excitation energy for ^{121}Sn. The corresponding predicted statistical values in the region above 10 MeV are found to be negligible. The weak ground state branching ratio (lower than 10%) measured below 8 MeV may be explained by the large mean spin value of states populated by the (α,^{3}He) reaction, as in the case of ^{91}Zr. In fact decay of the predicted [4] predominant (see Fig. 2) $i_{13/2}$ states by low energy neutrons is strongly inhibited by the centrifugal barrier. The ground state branching ratio drops rapidly with excitation energy to about 3×10^{-3} at 10 MeV, then tends to increase again. On the other hand, the branching ratio to the 2^+ state decreases with energy in a smoother way.

The angular correlations measured for the neutron decay of ^{121}Sn to the 0^+ ground state and lowest 2^+ state are shown in Fig. 9 (right). They are compared with the corresponding theoretical correlation functions, calculated assuming either a single initial 13/2 spin value (dashed line) or the distribution of spin values predicted by the BB calculations (full line). A qualitative agreement with the data is obtained using this second assumption.

B. The 6–14 MeV region in ^{65}Ni

Between the 6 MeV neutron emission threshold and 10 MeV in ^{65}Ni, the inclusive (α,^{3}He) spectrum of Fig. 1(c) displays a strong excitation of discrete levels. The corresponding final energy spectrum of neutrons is shown in Fig. 10(b). In addition to the branches to the ground state and 2^+ state at 1.34 MeV, one can clearly identify the transitions to the second 2^+ state at 2.28 MeV and the 4^+ state at 2.61 MeV.

The neutron spectrum shown in Fig. 10(a) corresponds to the decay of the 10–14 MeV energy range, where the inclusive spectrum of Fig. 1(c) displays a broad structure. According to the results of the semiclassical BB calculations (cf. Fig. 2). this structure may be due to the excitation of the $h_{11/2}$ single particle orbital. The neutron spectrum has been compared with the predictions of the statistical model.

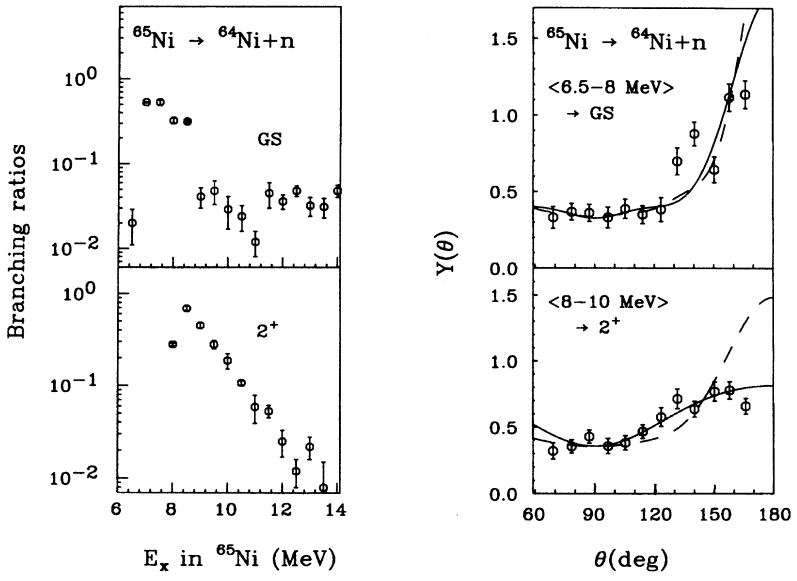

FIG. 11. Left part: neutron branching ratios to the ground state and first 2^+ state in ^{64}Ni, as a function of excitation energy in ^{65}Ni; right part: neutron angular correlations measured for the transitions to the ground state and first 2^+ state in ^{64}Ni, compared with the results of calculations for emitting states with relative J_a contributions predicted by the BB model (full lines) and one decaying state with J_a equal to 11/2 (dashed lines).

This comparison shows that the final low-lying levels of ^{64}Ni quoted above and other unidentified levels between 3 and 6 MeV are fed by a direct decay process. However, higher statistics data would be needed in order to get detailed information about these decay branches.

The branching ratios measured for the transitions to the ground state and lowest 2^+ state of ^{64}Ni energy in ^{65}Ni are displayed in Fig. 11 (left) as function of excitation energy. Large branching ratios are observed for the ground state transition between 7 and 8.5 MeV and for the 2^+ transition between 8 and 10.5 MeV excitation energy. This behavior is quite different from the one observed for ^{91}Zr and ^{121}Sn, preferentially decaying by γ-ray emission in a large energy range above the neutron emission threshold. This is readily explained by a lower centrifugal barrier as the available external orbitals in nickel have lower spin values than in the heavier nuclei.

The neutron angular correlations for the ground state and 2^+ transitions are compared in the right part of Fig. 11 with the results of the theoretical calculations described in Sec. III B. Using the initial BB spin distribution shown in Fig. 2, the calculated correlations are in rather good agreement with the data.

VI. DECAY OF THE HIGH-LYING CONTINUUM IN ^{65}Ni, ^{91}Zr, AND ^{121}Sn ($E_x > S_n + 8$ MeV)

A. Decay spectra

In this section we report the results obtained for the decay of the high-lying continuum states located between 8 and 16 MeV above the neutron emission threshold. Figure 12 displays the neutron decay spectra from four 2 MeV wide energy bins in ^{91}Zr, and Fig. 13 the spectra measured for the 14–18 MeV and 18–22 MeV excitation energy bins in ^{65}Ni and ^{121}Sn. These missing energy spectra clearly show the weak direct decay branches to low-lying states in the target nucleus. For the corresponding high-energy (above 10 MeV) neutrons, the resolution of EDEN only allows us to identify the well-resolved ground state without ambiguity in all the spectra.

More than 90% of the decay cross section for the three nuclei consists in low-energy neutrons, giving rise to a broad bump in the final energy spectra. The shape of these bumps is reproduced reasonably by the statistical calculations, performed according to the procedure presented in Sec. III C. In particular, the weak structures observed in the final energy spectra around 12 MeV in ^{90}Zr and 10 MeV ^{120}Sn and ^{64}Ni are accounted for by the statistical model. They correspond to the opening of the two-neutron emission decay channel.

On the other hand, a peak corresponding to the feeding of the ground state of the target nucleus is clearly observed in the high excitation energy spectra displayed in Figs. 12 and 13 for the three target nuclei. One also observes in the case of zirconium, a second peak centered around 2.7 MeV which could be tentatively assigned to the feeding of the lowest 3^- state. These transitions cannot be reproduced by the statistical calculations.

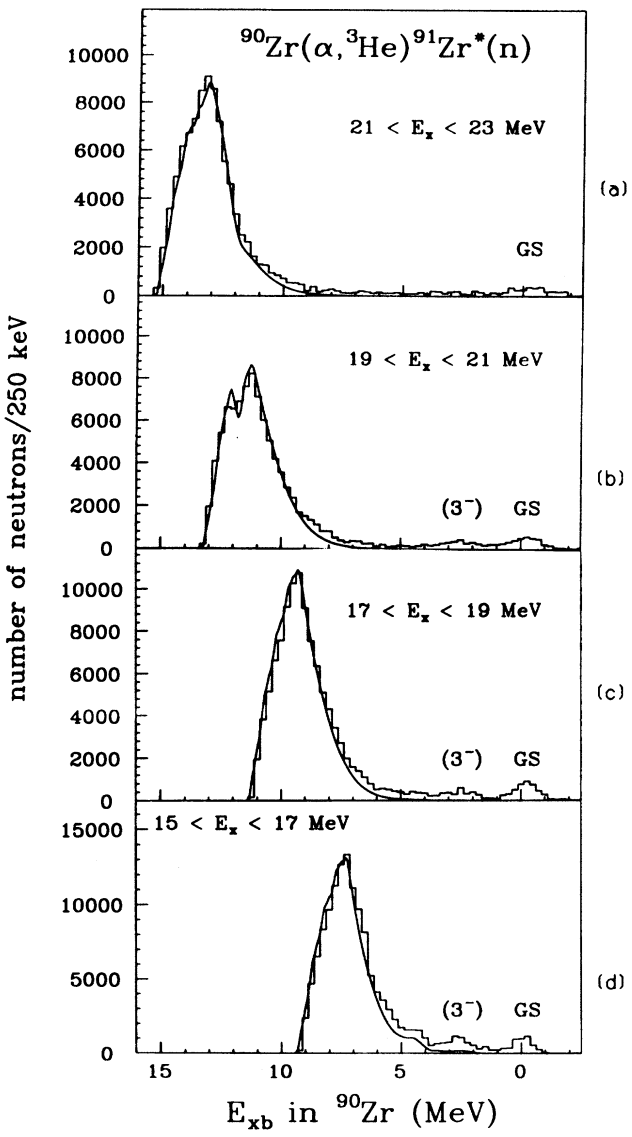

FIG. 12. Neutron spectra (histograms) from the decay of four energy bins in ^{91}Zr between 15 and 23 MeV excitation energy, displayed as a function of the energy of the residual ^{90}Zr nucleus. They are corrected for detector efficiency. Corresponding spectra predicted by statistical model calculations (solid lines) are also shown for comparison.

B. Angular correlations

The angular correlations measured for the low-energy neutrons emitted by the three nuclei under investigation, which correspond to the statistical bumps displayed in Figs. 12 and 13, are shown in the bottom parts of Fig. 14. They are found to be nearly isotropic, as expected for a statistical decay.

The neutron angular correlations measured for the ground state transition in the high excitation energy region are plotted in the upper part of Fig. 14. They are integrated over a 4 MeV energy bin, in order to get a significant statistical accuracy. These correlations exhibit an oscillatory behavior, with a dip at about 130° for Zr and Ni, and about 150° for Sn, and

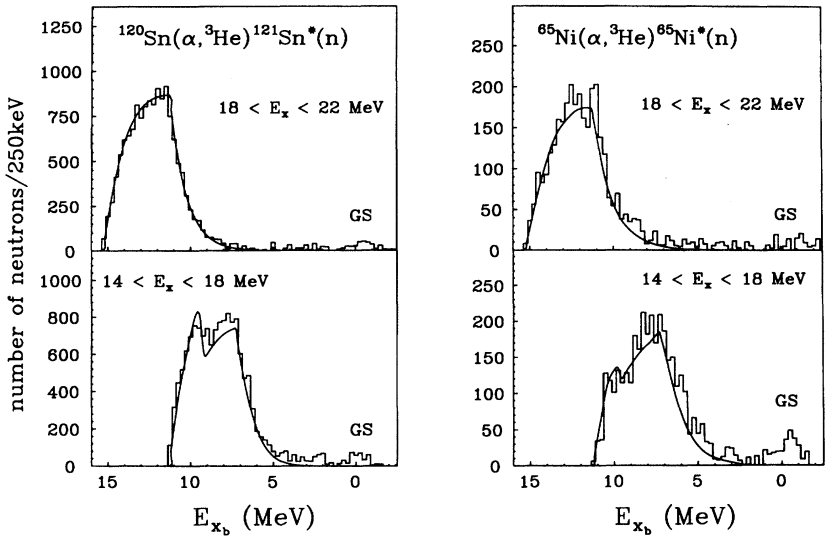

FIG. 13. Neutron spectra (histograms) from the decay of two energy bins between 14 and 22 MeV excitation energy in ^{121}Sn (left) and ^{65}Ni (right), corrected for detector efficiency and displayed as a function of the energy of the residual nucleus. Corresponding spectra predicted by statistical model calculations (solid lines) are also shown for comparison.

a peaking at 180°. Moreover, they clearly display an asymmetry relative to 90°. It is not possible to reproduce the angular correlations by the calculations described in Sec. III B for a pure (transfer+ neutron decay) process. These calculations have neglected possible interference between decaying states of different parities, which may give rise to 90° asymmetry, but such interference effects are expected to cancel over the 4 MeV wide energy interval. It is therefore very likely that the asymmetry is due to the elastic breakup process, which cannot be disentangled from ground state decay by kinematical considerations.

One can note that various models with different degrees of sophistication, such as the plane-wave Born approximation [27], the semiclassical model [28], the postform DWBA breakup theory [29], the quasifree breakup model [30], and the breakup fusion approach [31], have been proposed to calculate angular correlations resulting from breakup processes in several light ion induced reactions. The comparison of the present data with the predictions of these break-up models, applied to the $(\alpha,^{3}\text{He}\text{-}n)$ reaction, is beyond the scope of the present paper. Further measurements extended at more forward angles will certainly be useful in providing a stringent test for these calculations.

C. Neutron multiplicities

The measured multiplicities of neutrons detected in coincidence with ^{3}He particles are shown in Fig. 15 for the three nuclei under study. They correspond to neutrons with energy above the experimental threshold of 0.5 MeV. The dependence of the neutron multiplicities on excitation energy is compared with the predictions of the statistical model. Pro-

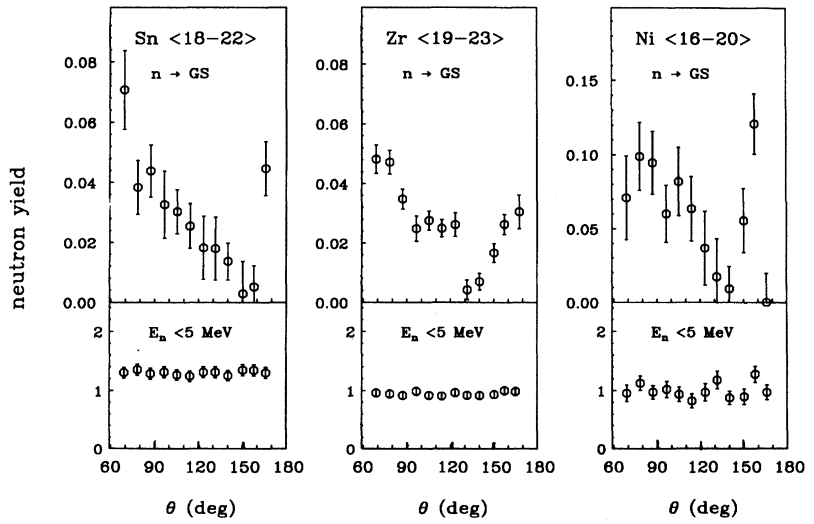

FIG. 14. Angular correlations of coincident neutrons observed in the region of the high-lying continuum.

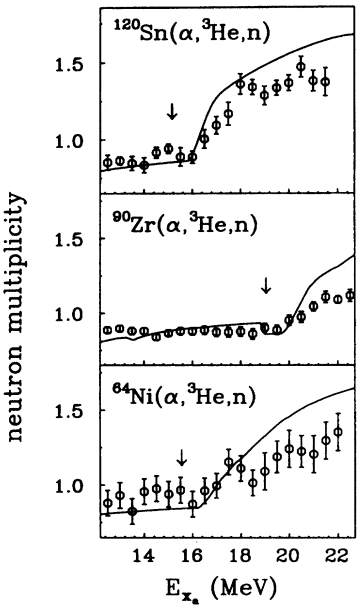

FIG. 15. Experimental neutron multiplicities above 0.5 MeV as a function of the excitation energy of the decaying nuclei ^{65}Ni, ^{91}Zr, and ^{121}Sn. The statistical model predictions are shown as solid lines; the arrows indicate the threshold energies S_{2n}.

ton emission is predicted to be completely negligible in ^{121}Sn and ^{65}Ni for the whole excitation energy range under study. As for ^{91}Zr, the proton branching ratio is predicted to be lower than 2% below the two-neutron energy threshold S_{2n}, and thus the total neutron multiplicity is found close to 1. The statistical multiplicity of neutrons above 0.5 MeV, which is displayed in Fig. 15, is in excellent agreement with the multiplicity of 0.88, measured between about 11 MeV and S_{2n}. One has to stress that the error bars displayed in Fig. 15 are only statistical and do not include the systematic relative uncertainty on the absolute efficiency, previously estimated to be less than 7%. The good agreement of calculated and experimental multiplicities below S_{2n} also observed for ^{121}Sn and—to a lesser extent—for ^{65}Ni gives confidence on the accuracy of the experimental branching ratios presented above.

The experimental multiplicity increases above S_{2n} in the three nuclei. However the values measured in the high excitation energy region are systematically lower than the predictions of the statistical model. This discrepancy is well established, since the calculated multiplicity was found to be nearly independent of any reasonable variation of the input parameters. This can be interpreted as experimental evidence for the existence of some "background" in the singles spectra, due to fast processes such as the breakup of the projectile. The neutrons associated with the "shape elastic breakup" are peaked at very forward angles [28] and thus may be largely undetected by the present setup where the EDEN cells are all located at angles greater than 68°.

As the experimental multiplicity was determined after normalization to the *total* singles cross section, whereas the calculated one corresponds to singles events due to the neutron transfer process, an approximate estimation of the contribution of transfer to the total (α,^{3}He) spectrum may be given by the ratio of these two numbers. At 21 MeV excitation energy, this ratio is equal to 0.86, 0.87, and 0.78 for ^{121}Sn, ^{91}Zr, and ^{65}Ni, respectively. These values are in qualitative agreement with the predictions of the BB model (0.82, 0.92, and 0.84, respectively [4]) at the same energy (see Fig. 2). From the present data, it is concluded that breakup processes producing undetected forward neutrons contribute for less than about twenty percent to the (α,^{3}He) cross section at high excitation energy.

VII. SUMMARY

The neutron decay of high-spin resonant states in ^{65}Ni, ^{91}Zr, and ^{121}Sn excited by the (α,^{3}He) reaction has been investigated using the multidetector EDEN, thus extending to lighter near-magic and semimagic nuclei the results previously reported in ^{209}Pb [12].

Nonstatistical decay modes in the three nuclei have been clearly observed in the region of the giant states, up to about 8 MeV above the neutron energy threshold. The decay characteristics of ^{91}Zr have been compared with the results of theoretical calculations performed using both the coupled-channel approach (CCA) [10] and the quasiparticle-phonon model (QPM). The conditions necessary for comparing experiment and theory in a meaningful way have been carefully examined. One of the sources of eventual difficulties is related to the uncertainties of the experimental "direct" (or semidirect) decay properties, extracted from statistical model calculations in a relatively low excitation energy region where some ambiguities exist. It is also necessary to make sure that the underlying nonresonant background not accounted for by the calculations (mainly due to transfer to low-spin states and breakup processes) can be neglected. The analysis of angular correlations has allowed us to check this particular point in the region of the 13 MeV giant state of ^{91}Zr.

The neutrons associated with the structureless continuum observed in the 8–16 MeV region above the neutron emission threshold in ^{65}Ni, ^{91}Zr, and ^{121}Sn have been also investigated. The analysis of the present data show that most of them are produced by the decay of high-lying states formed in the absorption process. The decay characteristics (angular correlations, neutron multiplicities) are consistent with an almost complete statistical damping, as it was previously observed in ^{209}Pb [12]. The contribution of the direct decay to the ground state could not be extracted in this energy region, due to the contamination of the projectile breakup. Further efforts will be needed to attempt to subtract this contribution, and confidently determine the ground state branching ratios corresponding to the direct decay of higher-lying unbound single-particle states.

ACKNOWLEDGMENTS

We wish to thank Dr. A. Bonaccorso, Dr. Nguyen van Giai, and Prof. M. Urin for communicating their results before publication and enlightening discussions. The help of M. Hofstee, Dr. J. Vernotte, S. van der Werf, and A. van der Woude at different stages of the experimental work is also gratefully acknowledged.

[1] G. Baur and T. Trautmann, Phys. Rep. C **25**, 294 (1976), and references therein.
[2] T. Udagawa, Y. J. Lee, and T. Tamura, Phys. Rev. C **39**, 47 (1989).
[3] A. Bonaccorso and D. Brink, Phys. Rev. C **44**, 1559 (1991).
[4] A. Bonaccorso, Phys. Rev. C **51**, 822 (1995).
[5] S. Gales, Ch. Stoyanov, and A. I. Vdovin, Phys. Rep. **166**, 127 (1988), and references therein.
[6] S. Fortier, S. Galès, S. M. Austin, W. Benenson, G. M. Crawley, C. Djalali, J. S. Winfield, and G. Yoo, Phys. Rev. C **41**, 2689 (1990).
[7] I. Lhenry, Ph.D. thesis, Université Paris XI, 1991; I. Lhenry *et al.* (to be published).
[8] N. Van Giai, Ch. Stoyanov, and V. V. Voronov, in *Selected Topics in Nuclear Structure,* edited by V. G. Soloviev (JINR, Dubna, 1994), p. 263.
[9] N. Van Giai, Ch. Stoyanov, V. V. Voronov, and S. Fortier, submitted to Phys. Rev. C.
[10] G. A. Chekomazov and M. H. Urin, Phys. Lett. B **349**, 400 (1995).
[11] H. Laurent, H. Lefort, D. Beaumel, Y. Blumenfeld, S. Fortier, S. Galès, J. Guillot, J. C. Roynette, P. Volkov, and S. Brandenburg, Nucl. Instrum. Methods **A326**, 517 (1993).
[12] D. Beaumel, S. Fortier, S. Gales, J. Guillot, H. Langevin-Joliot, H. Laurent, J. M. Maison, J. Vernotte, J. A. Bordewijk, S. Brandenburg, A. Krasznahorkay, G. M. Crawley, C. P. Massolo, and M. Renteria, Phys. Rev. C **49**, 2444 (1994).
[13] S. Fortier, in *Selected Topics in Nuclear Structure,* edited by V. G. Soloviev (JINR, Dubna, 1994), p. 269.
[14] A. G. Drentje, H. A. Enge, and S. B. Kowalski, Nucl. Instrum. Methods **122**, 485 (1973).
[15] J. M. Schippers, W. T. A. Borghols, and S. Y. Van der Werf, Nucl. Instrum. Methods **A247**, 467 (1986).
[16] C. P. Massolo, S. Fortier, S. Gales, F. Azaiez, E. Gerlic, J. Guillot, E. Hourani, H. Langevin-Joliot, J. M. Maison, and G. M. Crawley, Phys. Rev. C **43**, 1687 (1991).
[17] G. R. Satchler, *Direct Nuclear Reactions* (Oxford University Press, New York, 1983), p. 375.
[18] J. Van de Wiele (private communication).
[19] P. D. Kunz, code DWUCK4 (unpublished).
[20] J. Rapaport, V. Kuklarni, and R. W. Fulnay, Nucl. Phys. **A330**, 15 (1979).
[21] F. Puhlofer, Nucl. Phys. **A280**, 267 (1970); M. N. Harakeh, modified version of code CASCADE, private communication (1984).
[22] K. T. Knopfle and G. J. Wagner, in *Electric and Magnetic Giant Resonances in Nuclei,* edited by J. Speth (World Scientific, Singapore, 1991) and references therein.
[23] W. Dilg, W. Schantl, H. Vonach, and M. Uhl, Nucl. Phys. **A217**, 269 (1973).
[24] M. Maruyama, Nucl. Phys. **A131**, 145 (1969).
[25] D. Wilmore and P. E. Hodgson, Nucl. Phys. **55**, 673 (1963).
[26] Nucl. Data Sheets **67**, 639 (1992).
[27] N. Matsuoka, A. Shimizu, K. Hosono, T. Saito, M. Kondo, A. Sakaguchi, A. Goto, and F. Ohtani, Nucl. Phys. **A337**, 269 (1980).
[28] A. Bonaccorso and D. M. Brink, Int. Report No. 1PNO/TH 95-66, 1FUP-TH39/95, 1995 (unpublished).
[29] R. Shyam, G. Baur, F. Rosel, and D. Trautman, Phys. Rev. C **22**, 1401 (1980).
[30] E. H. L. Aarts, R. Malfliet, S. Y. Van der Werf, and R. J. de Meijer, Nucl. Phys. **A380**, 465 (1982).
[31] C. Y. Kim, T. Udagawa, J. Guillot, H. Langevin-Joliot, J. Van de Wiele, J. J. Florent, E. Hourani, E. Gerlic, and G. Duhamel, Phys. Rev. C **50**, 2935 (1994).